Advances in Aircraft and Spacecraft Science, *Vol. 11, No. 2 (2024) 195-213*
https://doi.org/10.12989/aas.2024.11.2.195

Effect of the stagnation pressure of a real gas on oblique shock waves

Mechta Mohammed*[1], Yahiaoui Toufik[1] and Dahia Ahmed[2]

[1]*Aeronautical Sciences Laboratory, Institute of Aeronautics, and Space Studies University of Blida 1, BP 270 Blida 09000, Algeria*
[2]*Nuclear Research Center of Birine, B.P 180, Ain Oussera 17200, Djelfa, Algeria*

(Received May 24, 2024, Revised July 13, 2024, Accepted August 10, 2024)

Abstract. This article deals with the changes in flow air properties across an oblique shock wave for a real gas. The flow through is investigated to find a general form for oblique shock waves. The main objective of this work will result in the development of a new numerical algorithm to determine the effect of the stagnation pressure on supersonic flow for thermally and calorically imperfect gases with a molecular dissociation threshold, thus giving a better affinity to the physical behavior of the waves. So, the effects of molecular size and intermolecular attraction forces are used to correct a state equation, emphasizing the determination of the impact of upstream stagnation parameters on oblique shock waves. As results, the specific heat pressure does not remain constant and varies with the temperature and density. At Mach numbers greater than 2.0, the temperature rise considerably, and the density rise is well above, that predicted assuming ideal gas behavior. It is shown that caloric imperfections in air have an appreciable effect on the parameters developed in the processes is considered. Computation of errors between the present model based on real gas theory and a perfect gas model shows that the influence of the thermal and caloric imperfections associated with a real gas is important and can rise up to 16%.

Keywords: normal shock wave; oblique shock wave; perfect gas; real gas; supersonic air flow

1. Introduction

A variety of compression flow problems have been investigated under the assumption that air behaves like an ideal gas. This assumption is justified since the pressure and temperature range of interest is small and near atmospheric. This hypothesis is experimentally proven, however, that when air is subjected to large changes in state at pressure and temperature far away from atmospheric, it obeys other laws and properties other than those of ideal gases. Hence, such flows will be encountered in supersonic wind tunnels and by aircraft flying at high supersonic airspeeds. The nature and extent of this departure have become important considerations in aerodynamics.

The classical theories backed by experiments demonstrate that there are three parameters in real gas properties that cause a change in their properties differently from the perfect gas. These parameters can be set to have thermal and caloric imperfections. Thermal imperfections characterizing intermolecular forces and molecular size effects react significantly at low temperatures and pressures. This is not the case at high temperatures where changes in vibrational

*Corresponding author, Ph.D. Student, E-mail: mechta_mohammed@univ-blida.dz

http://www.techno-press.org/?journal=aas&subpage=7 ISSN: 2287-528X (Print), 2287-5271 (Online)

capacities cause caloric imperfections, conditions in which the effects of molecular dissociation and electronic excitation become significant (e.g., temperatures significantly above 3550 K).

The thermal and calorific imperfections influence the behavior of supersonic air flows and, in particular, all thermodynamic and physical parameters. The Normal Shock Wave (NSW), Oblique Shock Wave (OSW), and Conical Shock Wave (CSW) are a multi-physical phenomenon that appears in nature only for supersonic flows when some specific conditions are applied (Anderson 1982, Goldsmith and Seddon 1999, Sutton and Biblarz 2010). A shock wave is a flow zone of very small thickness where it is a transition between upstream fluid flow, where the speed is supersonic, and downstream fluid flow, where the speed is subsonic. In this zone, the particles of the flow crossing the shock wave with an extremely strong deceleration. Shock waves can propagate either in the normal direction of the flow or obliquely, referred to as normal shock waves or oblique shock waves, respectively.

Modeling the detonation of aluminum particles in air is a very difficult task to achieve because the combustion phenomenon is shock induced and there is multiphase heat release and transfer in supersonic flows. Air is frequently used as a gas in external and internal propulsion flows for all aeronautical, aerospace, or even wind tunnel applications, especially for shock wave calculations, as it exists in nature (Tatum 1997, Maccoll 1937, Sims 1964).

In recent years, the authors of references (Anderson 1982, Goldsmith and Seddon 1999, Sutton and Biblarz 2010, Tatum 1997, Maccoll 1937, Sims 1964, Agnone 1994) have designed studies of NSW, OSW and CSW using calorically ideal gases, where the CP is constant and does not depend on the temperature.

It gives good results for low T_0, M_1 and θ, which do not exceed 240 K, 2.00 and 10 degrees, respectively. This model for gas is called the PG model.

The authors in reference (Tarnavskii 2004) investigated the possibility of dualistic solutions to the problem of shock wave patterns of reflection of two different types at the same diagnostic variables, such as regular or Mach reflection (Neumann paradox), in the air intakes and nozzles of engines of hypersonic aircraft in certain ranges of flight conditions. The creation of a mechanism for adjusting the entry of the flow into the diffuser is required for the hypersonic ramjet engine (HRE) to function under planned parameters.

In reference (Rodio *et al.* 2014) to applying the suggested method to a specific application, the simulation of a rarefaction shock wave (RSW) in a multiphase flow, demonstrate how the numerical solver based on a DEM formulation may be updated to accommodate more sophisticated equations of state for the vapor region. In order to comprehend the impact of not having extremely exact knowledge of the EOS coefficients on the structure of the solutions, we will explore the coupling of this method with uncertainty quantification tools.

In reference (Gupta and Sharma 2017) they identify a group of solutions to the shock wave affected, unsteady 2 dimensional flow of a van der Waals fluid, and construct an asymptotic amplitude equation with cubic and quadratic nonlinearities, including dissipation and diffraction. We have demonstrated how the van der Waals parameters a and b, which represent the true gas effects, have an impact on the shock's shape, strength, and decay pattern.

In reference (Navarro 2019) they found that the downstream circumstances of a typical shock were explained, two unique approaches were explained, and the outcomes were compared to ideal gas solutions. The cubic equation of state was solved using computer code.

To examine the effects on the real gas solutions, a broad range of stagnation temperatures and pressures were explored. Following the result's tabulation, it was determined that the majority of solutions have the greatest value for ideal gas solutions when their stagnation temperatures and

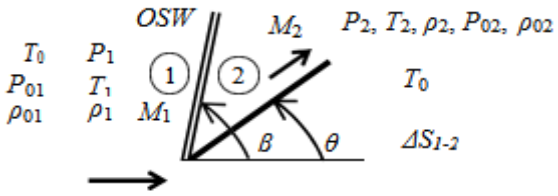

Fig. 1 Oblique shock wave illustration

pressures are lower and higher, respectively.

In reference (Ali 2023) they numerically examined some physical characteristics in the presence of an oblique shock wave. For the three different Mach numbers, velocity, turbulent viscosity, total pressure, and total enthalpy have all been studied upstream and downstream of the shockwave. According to the findings, the total pressure downstream of the shock wave was lower than the total pressure upstream. Additionally, as the Mach numbers increase, the turbulent viscosity region around the item thickens. In addition, the overall pressure varied slightly throughout the three Mach levels. The shock wave effects are re sponsible for these behaviors of the aforementioned parameters. Additionally, it appeared that the oblique shock wave angle dropped as the Mach number grew.

In the light of the above listed references, the aim of this work is to develop a new mathematical model and a numerical calculation tool (calculator) to determine the effects of stagnation pressure on supersonic flow, using the equations of an oblique shock in case of a perfect and real gas, calorically and thermally imperfect, below the dissociation threshold of the molecules. In order to correct the Perfect gas (*PG*) model and determine the thermodynamic parameters presented by the density ratio, the pressure ratio, the temperature ratio, the downstream Mach number, and the entropy as a function of the upstream Mach number are largely treated. In this case, the specific heat at constant pressure does not remain constant and varies with increasing temperature.

2. Mathematical formulation

The shock is characterized by the determination of the thermodynamic parameters and the Mach number through the shock, as well as by the increase in entropy. For this, the goal of this work is to develop the necessary thermodynamic and geometric ratio relationships and to study supersonic isentropic flow using oblique shock equations in the case of a real, thermally imperfect gas.

Fig. 1 represents a general diagram of an *OSW* on a dihedral inclined by an angle θ and the envisaged parameters.

To determine the specific thermodynamic parameters (M_2, β, T_2/T_1, ρ_2/ρ_1, P_2/P_1, P_{02}/P_{01} and ΔS2-1) through OSW (Kenneth 1996, Kenneth 1997), the first step consisted to improve the HT model presented in References: Tatum (1997), Kenneth (1996), Kenneth (1997), Zebbiche (2009). After correcting the relationship between β, θ and $M1$. Since the authors in these references used equations designed for the PG model at constant CP, due to difficulty in finding an analytic form, the results are find far from reality and not suitable for the operation of the RG model. The said equations are the most interesting ones in computing OSW parameters since all other parameters

depend on, β, θ and M_1. The relationships are summarized by the equations below (Elaichi and Zebbiche 2018, Bounjad *et al.* 2017)

$$\frac{\rho_2}{\rho_1} = \frac{tg(\beta)}{tg(\beta-\theta)} \tag{1}$$

$$P(T,\rho) = \frac{\rho RT}{(1-\rho b)} - a\frac{\rho^2}{T} \tag{2}$$

The energy equation in differential form is written by

$$dH = C_P dT + \left(\frac{\partial H}{\partial P}\right)_T dP \tag{3}$$

Using the thermodynamic relationship, we can determine, after mathematical transformations, for the Berthelot's equation the following relationship

$$\left(\frac{\partial H}{\partial P}\right)_T = C_T = \left(\frac{3ab^2\rho^2-6ab\rho-RT^2b+3a}{2ab^2\rho^3-4ab\rho^2+2a\rho-RT^2}\right) \tag{4}$$

The differential of Berthelot's equation is

$$dP = \left(\frac{RT^2-2a\rho(1-b\rho)^2}{T(1-b\rho)^2}\right) d\rho \tag{5}$$

Replacing Eq. (5) into Eq. (3), we have

$$dH = C_P(T,\rho)dT + C_T(T,\rho)d\rho \tag{6}$$

The energy equation in differential form between the velocity and the enthalpy therefore gives the following relationship

$$V(T,\rho)dV = -C_P(T,\rho)dT - C_T(T,\rho)d\rho \tag{7}$$

The expressions $V(T, \rho)$, $CP(T, \rho)$, $CT(T, \rho)$ and $SV(T, \rho)$ are presented in Refs: (Xiang *et al*. 2019, Salhi and Roudane 2019, Salhi *et al*. 2016).

$$C_P(T,\rho) = \frac{\gamma_{PG}R}{(\gamma_{PG}-1)} + R \times \left\{ \left(\frac{\theta}{T}\right)^2 \frac{e^{\frac{\theta}{T}}}{\left(1-e^{\frac{\theta}{T}}\right)^2} + \frac{2a\rho}{RT^2}\left[1 + \frac{\left(\frac{2-b\rho}{1-b\rho}+\frac{a\rho}{2RT^2}\right)}{\frac{1}{(1-b\rho^2)}-\frac{2a\rho}{RT^2}}\right] \right\} \tag{8}$$

$$C_T(T,\rho) = \frac{3ab^2\rho^2-6ab\rho-RT^2b+3a}{2T\rho b-Tb^2\rho^2-T} \tag{9}$$

$$S_V^2(T,\rho) = \frac{RT}{(1-b\rho)^2} - \frac{2a\rho}{T} + \frac{\rho^2 T\left(\frac{a}{T^2}+\frac{R}{\rho(1-b\rho)}\right)^2(\gamma_{PG}-1)}{R\left[1+(\gamma_{PG}-1)\left\{\left(\frac{\theta}{T}\right)^2\frac{e^{\frac{\theta}{T}}}{\left(1-e^{\frac{\theta}{T}}\right)^2}+\frac{2a\rho}{RT^2}\right\}\right]} \tag{10}$$

Combining Eqs. (7) and (10) yields the following equation for the Mach number

$$M(T,\rho) = \frac{V(T,\rho)}{S_V(T,\rho)} \tag{11}$$

In thermodynamics, all state parameters can be defined by two state variables: (Xiang. *et al*. 2019, Salhi and Roudane 2019, Zebbiche 2019), chosen by T and ρ in our study. From the differential form: (Xiang *et al*. 2019, Salhi and Roudane 2019, Thompson 1995, Van Wylen

1973), the Bernoulli Equation can be written by

$$VdV + S_V^2 \frac{d\rho}{\rho} = 0 \tag{12}$$

Replacing Eq. (7) into Eq. (12), we obtain

$$\frac{d\rho}{\rho} = \frac{C_P(T,\rho)}{S_V^2} dT + \frac{C_T(T,\rho)}{S_V^2} d\rho \tag{13}$$

$$E^{(T)} dT = E^{(\rho)} d\rho \tag{14}$$

$$E^{(T)} = \frac{C_P(T,\rho)}{S_V^2(T,\rho)} \ , \ E^{(\rho)} = \frac{1}{\rho} - \frac{C_T(T,\rho)}{S_V^2(T,\rho)} \tag{15}$$

The Entropy equation on the shock

$$dS = \frac{C_P(T,\rho)}{T} dT - \frac{\upsilon}{T} dP \tag{16}$$

The relationship between v and ρ is

$$\upsilon = \frac{1}{\rho} \tag{17}$$

For Eq. (2) we can write

$$dP = \frac{RT^2 - 2a\rho(1-b\rho)^2}{T(1-b\,\rho)^2} d\rho \tag{18}$$

Replacing both Eqs. (17) and (18) into Eq. (16), we have

$$\Delta S_{2-1} = \int_{T_{01}}^{T_{02}} S^{(T)} dT - \int_{\rho_{01}}^{\rho_{02}} S^{(\rho)} d\rho \tag{19}$$

$$S^{(T)} = \frac{C_P(T,\rho)}{T} \ , \ S^{(\rho)} = \frac{RT^2 - 2a\rho(1-b\rho)^2}{\rho T^2 (1-b\rho)^2} \tag{20}$$

3. Numerical procedure

In the reverse resonance, the cone deviation that coincides with the shock is determined. In reality, the cone deflection is given and the corresponding shock must be determined with the two main parameters, which are β (shock angle) and M_1 (Mach number) for a given air temperature T_0. In this context, we need to know the variation of C_P (T, ρ) as a function of air temperature, density, and constant R.

To achieve this work, the first step consists to determine all isentropic parameters (T_1/T_0, ρ_1/ρ_0, P_1/P_0) corresponding to M_1 and T_0 just before the shock, of course using the relations for isentropic supersonic flow (Anderson 1989, Salhi and Roudane 2019). Therefore, the second step is to determine the properties of the flow through the shock, which are summarized by (M_2, θ, T_2/T_1, ρ_2/ρ_1, P_2/P_1, P_{02}/P_{01}, $\Delta S_{2\text{-}1}$). We use the relations of an oblique shock wave at RG, which are presented respectively by Eqs. (1) to (5), up to (20). These static parameters can be determined once the Mach number M1 is known, by solving the system of nonlinear algebraic equations created by Eqs. (2), (7), (8), (10), (11), (13) and (20). Using Eqs. (2), (7), (8), (10), (11), (13) and (20), first with temperature and then with density, the calculation is performed using Newton's algorithm (Salhi *et al.* 2016).

Two solutions can be found depending of the Mach number M_2 just after the shock. This

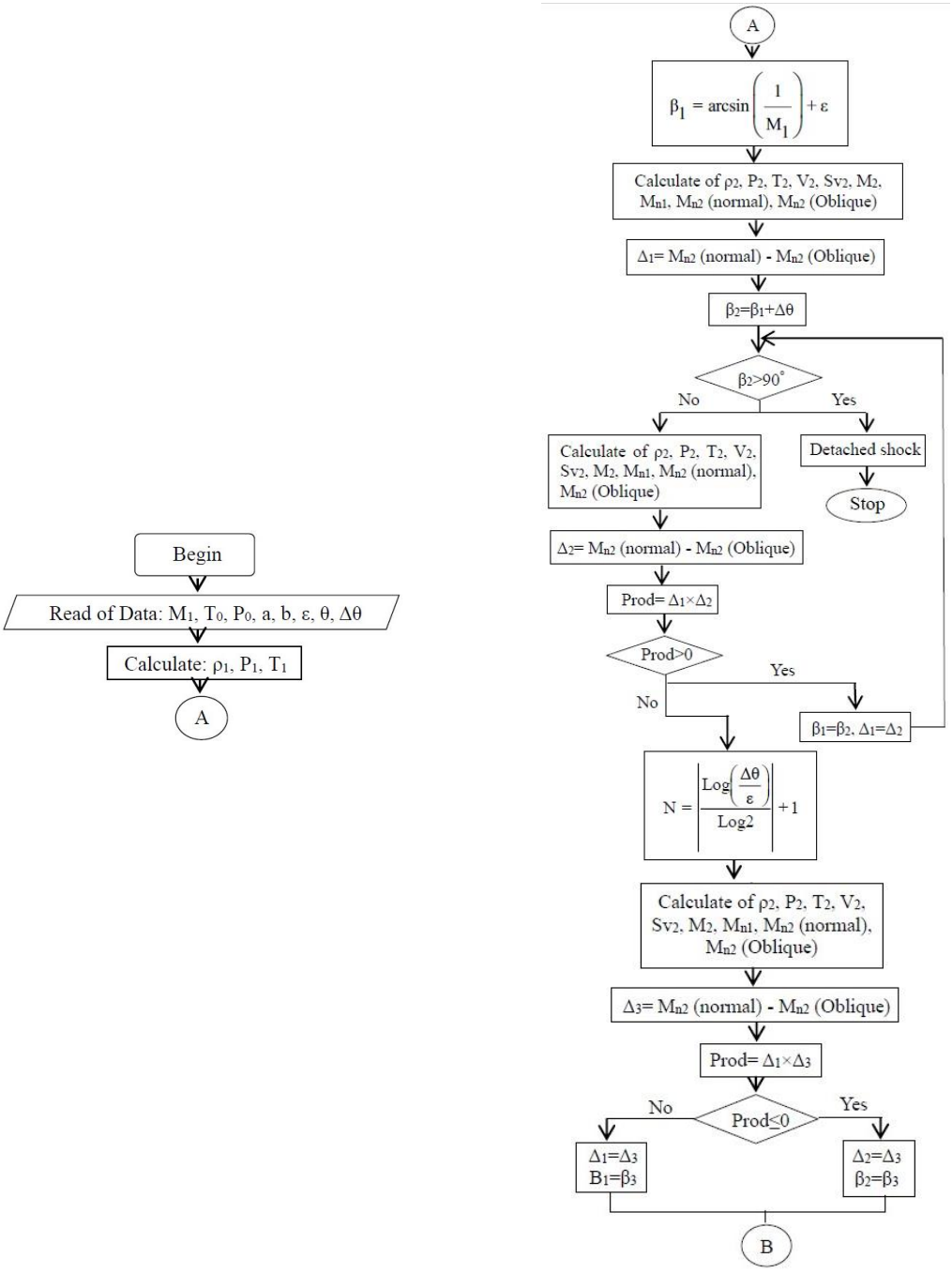

Fig. 2 Numerical algorithm to calculate air flow properties across an oblique shock wave

implies that all thermodynamic parameters will admit two solutions, If $M_2 \geq 1.00$, we get a weak shock. If $M_2 < 1.00$, we get a strong shock. The weaker shock is the one that actually occurs. Before deter-mining the parameters presented in relations (1) to (5), up to (20), it is firstly necessary to

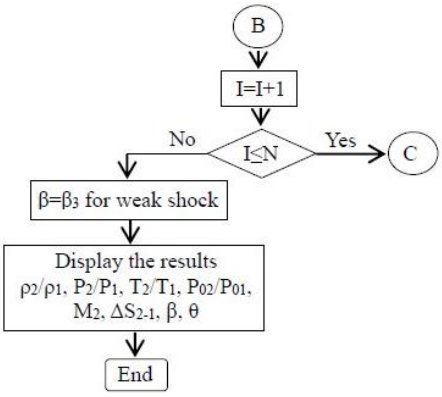

Fig. 2 Continued

determine the flow deviation θ just after the shock. In references (Peterson and Hill 1965, Zebbiche 2019), the authors used the relation for a perfect gas at constant C_P, given the difficulty of finding an analytical form. This gives results that are far from the reality and do not meet the needs of the RG case. We will determine the deviation θ with high accuracy according to the RG model. All the parameters just after the shock depend directly and explicitly on the value of θ. As the development of an analytical relationship, linking the parameters β and θ is rather complicated. We will use the relations of a normal shock wave to RG to determine the value of M_2 :(Thompson 1995, Van Wylen 1973).

To achieve our goal, a numerical algorithm was developed using FORTRAN, a programming language suitable for numeric calculations such as the ones required for the shock relations (see Fig. 2). For a given free stream airflow, the program can calculate flow properties behind a normal and/or an oblique shock wave, as well as in a sequence of oblique shock waves, for both air gas models: perfect gas and real gas. For calculations of flows in a sequence of oblique shock waves, the flow shock angle β for each shock wave should also be given. Regardless of the gas model considered, free stream airflow is treated as a calorically perfect gas for which Mach number, pressure, and temperature are provided. Since the program deals with atmospheric air, values are γ=1.4 and R=287 (J/kg.K). The following calorically perfect and shock relations can be found in Ref: (Anderson 1982, Anderson 1989).

4. Error caused by the PG model

The *PG* model is developed on the basis of considering the specific heat C_P constant, which gives acceptable results for low T_0, M_1 and β. According to this investigation, a difference in the results given between the *PG* model and our *RG* model will be presented. The error given by the *PG* model with respect to our *RG* model can be calculated for each parameter. However, for each value of T_0, M_1 and β, the error ε can be evaluated using the relation below

$$\varepsilon = \left|1 - \frac{Parameter_{PG}}{Parameter_{RG}}\right| \times 100 \tag{21}$$

Where the parameters *PG* and *RG* represent the values of parameters calculated by the *PG* and *RG* models, respectively.

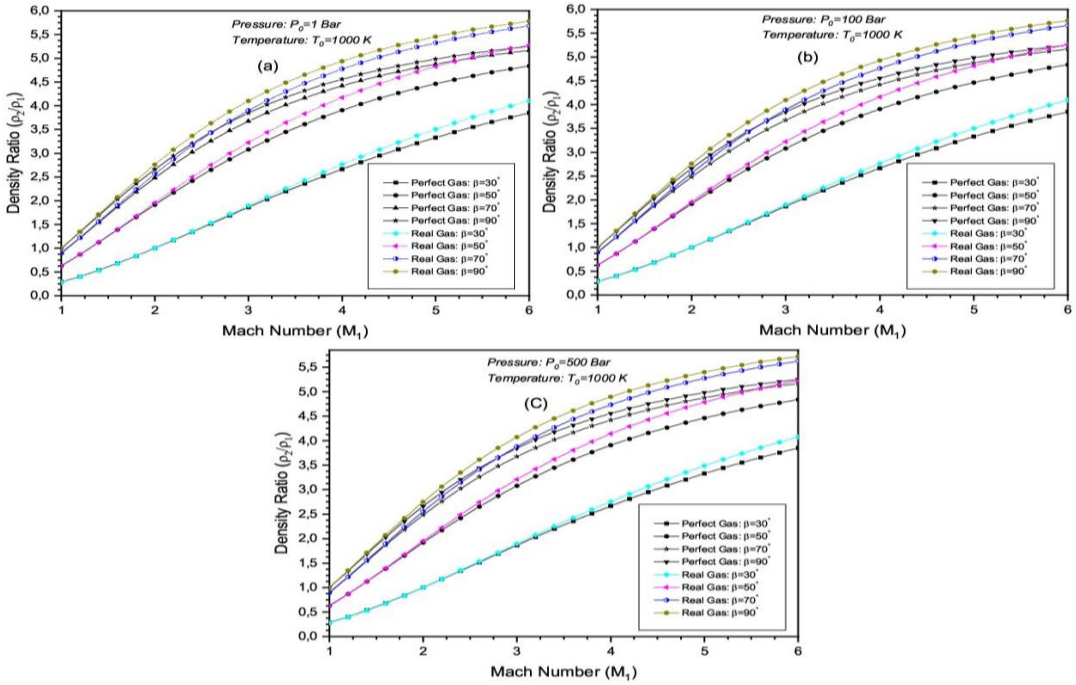

Fig. 3 Variation of ρ_2/ρ_1 through an oblique shock wave versus M_1

5. Results and discussions

In this section, we present our results with their interpretations. We have divided the results into two parts to make it easier for the reader. All the obtained results are a function of four main physical data parameters: M_1, T_0, P_0, and β. notably, our application is made for air. The convergence of the results depends on the discretization, which is reflected in the choice of step used in Newton's method. However, our program can handle any type of gas, despite the fact that we used the C_P (T, ρ) and R functions for air only. In the applications, we took a step Δx=0.001 after several convergence tests to get an accuracy of ε=10^{-4}.

Given the change made to the mathematical model, this modification is found in the relationship that links shock deflection and dihedral deflection as well as in the interpolation of C_P (T, ρ) for the reason of modeling the RG model with high accuracy.

5.1 Variation of density ratio for a given upstream Mach number

Fig. 3 shows the variation of density ratio (ρ_2/ρ_1) across oblique shock waves as a function of upstream Mach number, as well as the stagnation pressures P_0=1 bar, 100 bar, and 500 bar, at constant stagnation temperature T_0=1000 K, and different values of oblique shock angle β for *PG* and *RG* models. We can see that the variation of the density ratio clearly depends on the cited parameters. The effect of the stagnation pressure on the density ratio is apparent, where the increase of P_0 causes an increase in the mass density further if M_1 and β increase linearly.

The curves are approximately have the same shape, and there are a slight difference between *PG* and *RG* models. The gap between the two models starts to increase once the Mach number

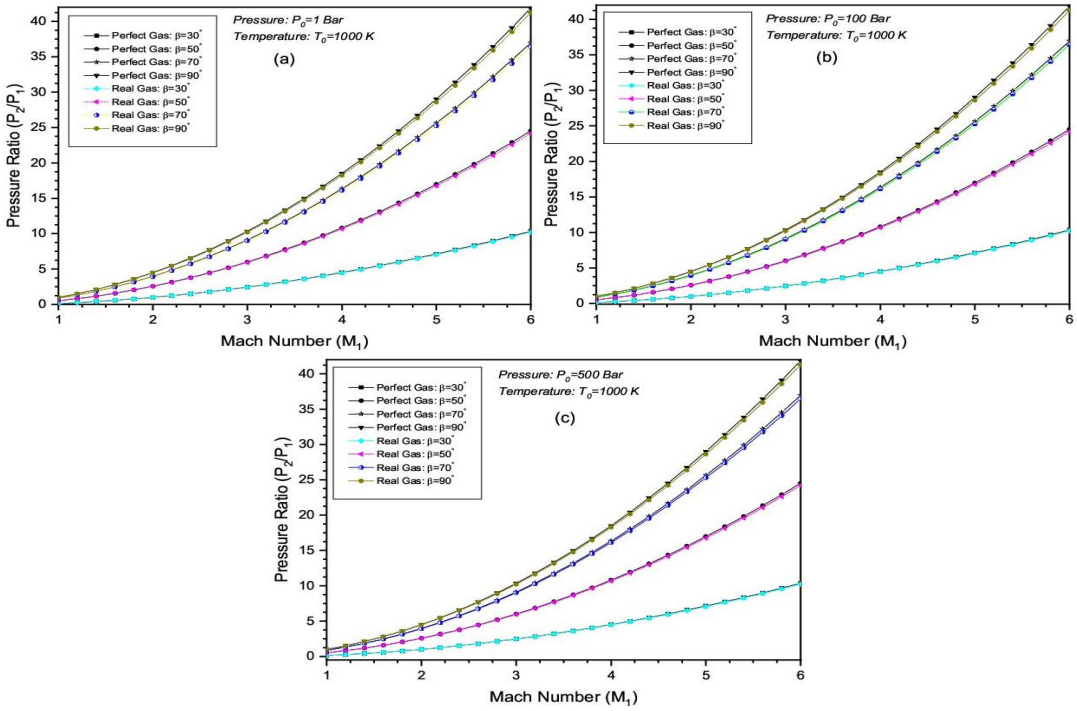

Fig. 4 Variation of P_2/P_1 through an oblique shock wave versus M_1

increases, and the results obtained by the *RG* move away from those obtained by the *PG* model. Thus, this variation demonstrates the effects of molecular size and intermolecular force bound by Berthelot's equation. As illustration:

In the *PG* model, M_1=1.6, and β=30°, ρ_2/ρ_1=0.6819753 for P_0=1 bar, P_0=100 bar, and P_0=500 bar. In the *RG* model, by considering the same conditions, the rapport of density ρ_2/ρ_1 is equal to 0.6773061 for P_0=1, 0.6774424 for P_0=100 bar, and 0.677858 for P_0=500 bar.

By considering β=50°, the density ratio for the PG model, take a value of 1.387824 for P_0=1 bar, for P_0=100 bar, and for P_0=500 bar. In case of the RG model, ρ_2/ρ_1=1.398862 for P_0=1bar, 1.398515 for 100 bar, and 1.39764 for 500 bar.

The density ratio for the PG model, by corresponding β=70°, ρ_2/ρ_1=1.867704 for P_0=1 bar, for P_0=100 bar, and for P_0=500 bar. In the RG model, ρ_2/ρ_1 will be 1.90351, for P_0=1 bar, 1.902439 for P_0=100 bar, and 1.899746, for P_0=500 bar.

5.2 Variation of the pressure ratio for a given upstream Mach number

Fig. 4 represents the variation in pressure ratio (P_2/P_1) across oblique shock waves versus the upstream Mach number for some values of the pressure P_0 and stagnation temperature T_0=1000 K using *RG* and *PG* models. From the found results, we can see that the increase in stagnation pressure causes an increase in the pressure ratio from 0 to a height number for both models. The curves, which almost take the similar form, are completely superimposed and there is no gap of each case. As example, for the *PG* and *RG* models, giving T_0=1000 K and β=30°, the pressure ratio will be 0.4147315 for P_0=1 bar, 0.4144616 for P_0=100 bar, and 0.4137815 for P_0=500 bar.

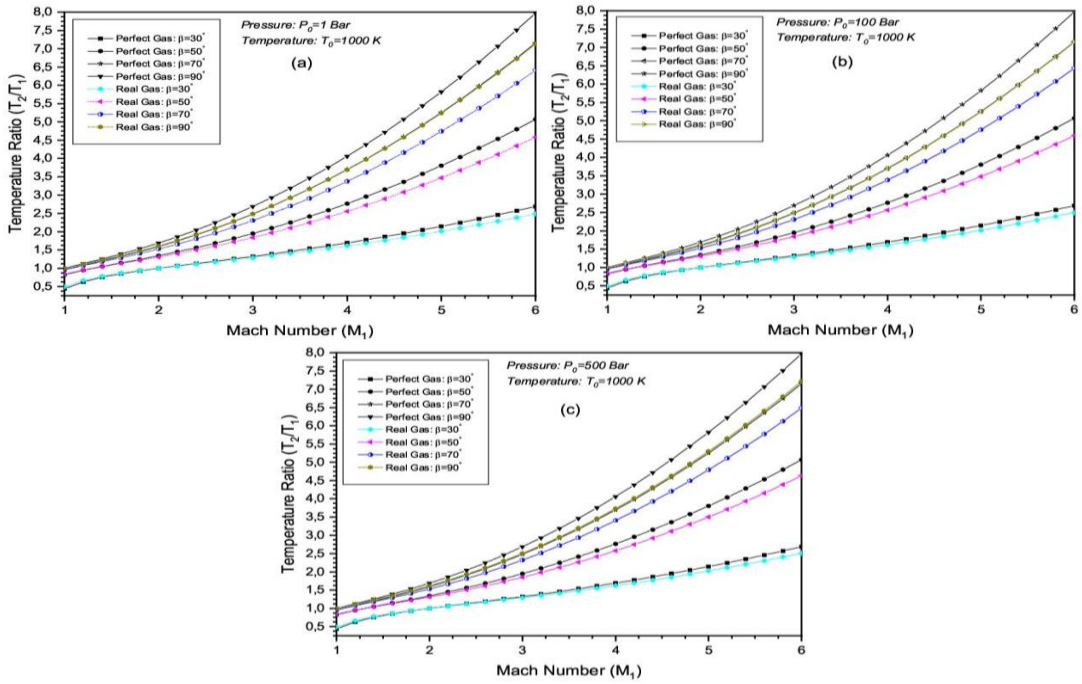

Fig. 5 Variation of T_2/T_1 through an oblique shock wave versus M_1

Whereas, if M_1 increase more 2.00 and β>30°, the stagnation pressure P_0 increases the pressure ratio (P_2/P_1) simultaneously.

We infer that the flow velocity increases in oblique shock waves if the upstream Mach number increases, which results in an increase in the pressure ratio.

5.3 Variation of the temperature ratio for a given upstream Mach number Mach number

Fig. 5 shows the variation in temperature ratio (T_2/T_1) across oblique shock waves as a function of upstream Mach number, as well as certain stagnation pressures P_0=1 bar, 100 bar, and 500 bar, stagnation temperature T_0=1000 K for *PG* and *RG* models. We can see that the variation of the temperature ratio clearly depends on P_0, T_0, M_1, and β. We can also see the effect of T_0 and P_0 on the temperature ratio and the gap between the *PG* and *RG* models, which increases further if M_1 and β increase gradually. For M_1<2.00 and β=30.0 degrees, if P_0 increases, the temperature ratio (T_2/T_1) decreases slightly for each given value of T_0, if T_0 increases, the temperature ratio (T_2/T_1) decreases slightly for each given value of P_0. The curves of Fig. 4 are approximately coincident (with precision).

For the *PG* model, if M_1=1.8, β=30°, the temperature ratio take a values of 0.9307084 for P_0=1 bar, 100 bar and P_0=500 bar. In the case of *RG* model 0.9380628 for P_0=1 bar, 0.9378464 P_0=100 bar and 0.9373012, for P_0=500 bar,

For the *RG* model, if M_1<2, β=>30°, with respectively the corresponding pressures of 1 bar, 100 bar, and 500 bar, we can see that the temperature ratio (T_2/T_1) is inversely proportional to T_0, when T_0 increase (T_2/T_1) decreases slightly for every value of P_0, and β. If P_0 and β increases, the

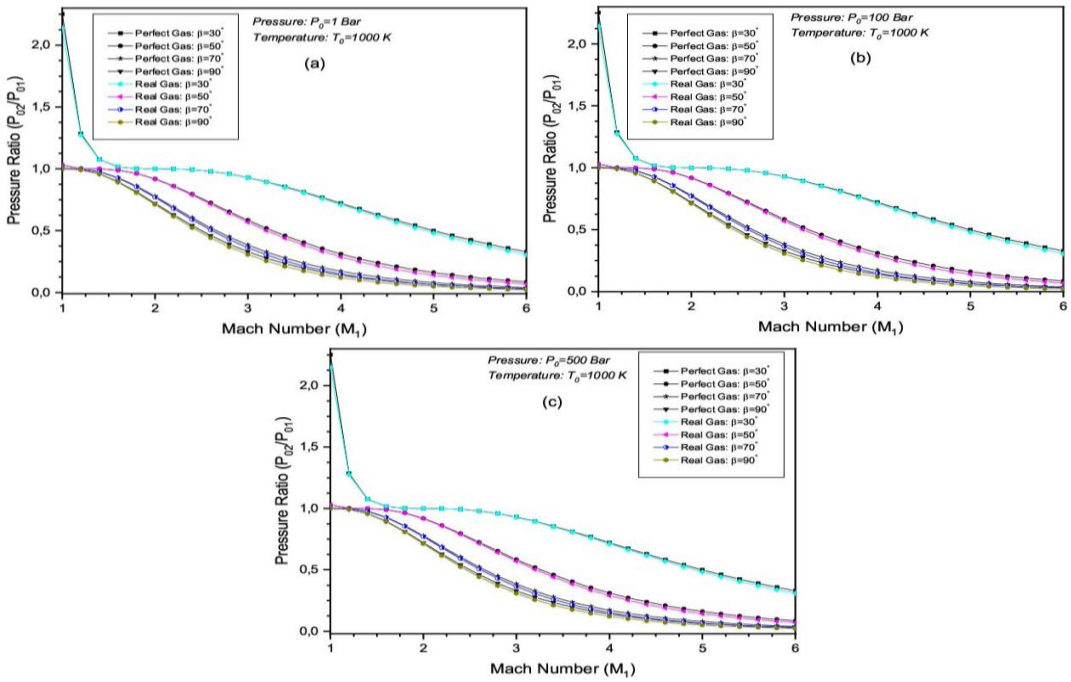

Fig. 6 Variation of P_{02}/P_{01} through an oblique shock wave versus M_1.

temperature ratio (T_2/T_1) increases slightly, the flow velocity rises if the upstream Mach number rises, causing the temperature ratio to rise.

We draw the conclusion that in oblique shock waves, the variation of the temperature ratio obtained by the *Real Gas* are always lower than those obtained by the *Perfect Gas* indicating the real thermodynamic behavior of the gas.

5.4 Variation of the total pressure ratio of oblique shock waves for a given upstream Mach number

Fig. 6 shows the variation in total pressure ratio (P_{02}/P_{01}) of oblique shock waves as a function of upstream Mach number. Contrary to the results of the pressure ratio cited in paragraph 5.2, we can see that both models take the same shape of decreasing, the total pressure ratio values are low at big values of Mach number. However, the total pressure ratio decreases with a height value of P_0, increase slightly, then linearly decrease for any increase in the shock angle deviation β.

5.5 Variation of downstream Mach number of oblique shock waves for a given upstream Mach number

The influence of the stagnation conditions on downstream Mach number (M_2) through an oblique shock wave versus the upstream Mach number (M_1) are shown in Fig. 7. As seen, there is a decrease then an increase in downstream Mach number (M_2) further if M_1<2 and β=30°. If β increases, the downstream Mach number increases slightly for every value of T_0 and P_0 and becomes constant at β=90°.In comparison between the two models, we remark that there is little

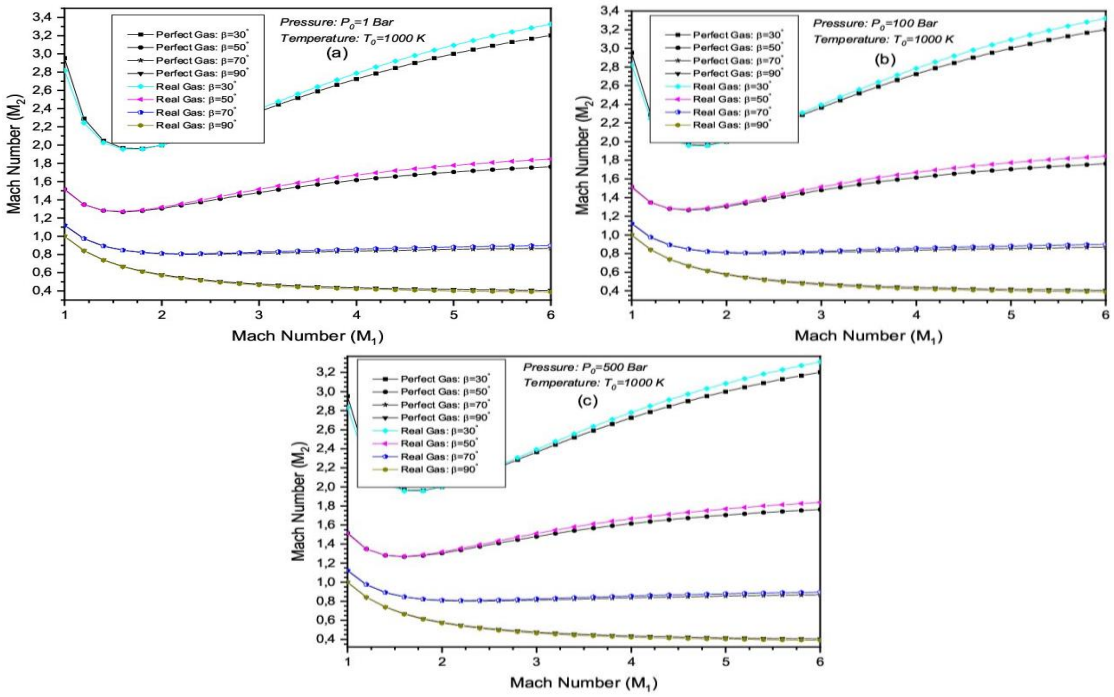

Fig. 7 Variation of M_2 through an oblique shock wave versus M_1

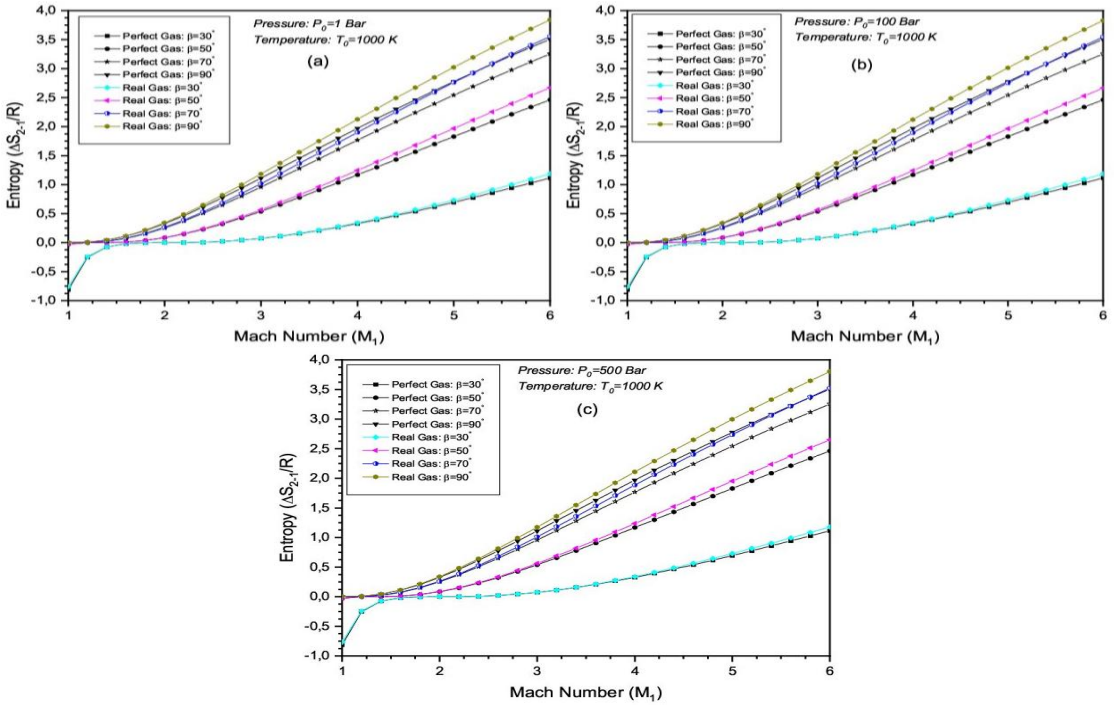

Fig. 8 Variation of ΔS through an oblique shock wave versus M_1

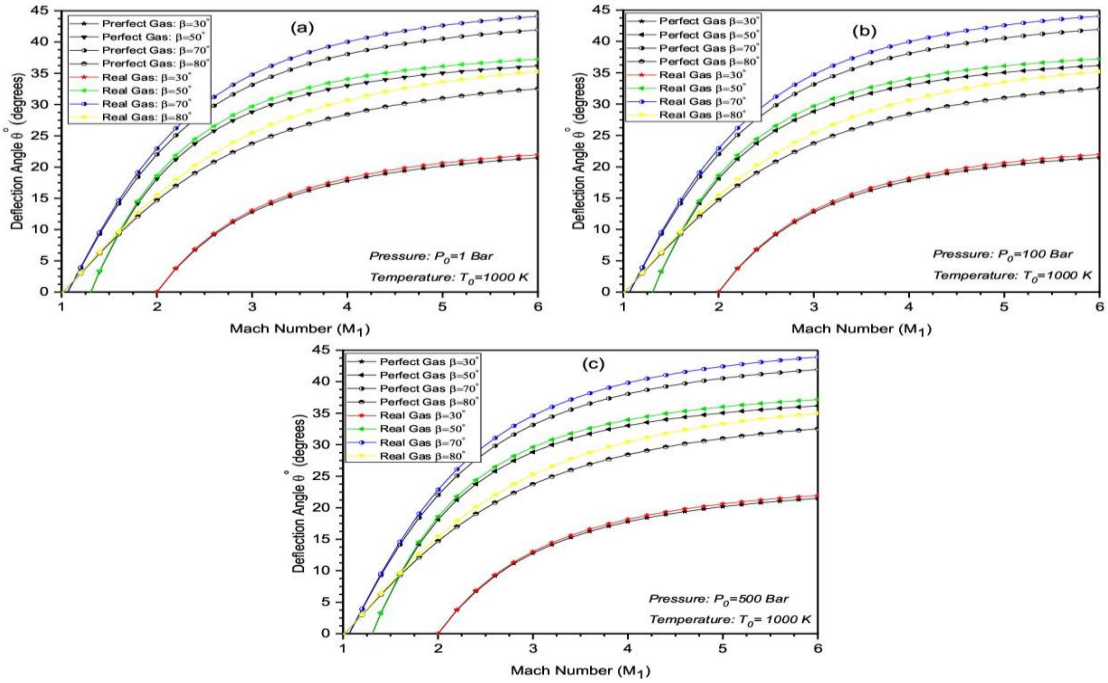

Fig. 9 Variation of θ through an oblique shock wave versus M_1

gap between the two shapes, the maximum error is estimated to 3.27% (Table 2).

5.6 Variation of the Entropy for a given upstream Mach number

Fig. 8 shows the variation in the entropy ($\Delta S_{2\text{-}1}/R$) across oblique shock waves versus the upstream Mach number until the stagnation pressures P_0=1 bar, 100 bar, and 500 bar for the above cited conditions of temperature and deviation angle β considering the PG and RG models. After calculation, we found at a low value of Mach number and for each given value of β, the entropy ($\Delta S_{2\text{-}1}/R$) is very low then becomes significant when the value of Mach number is too high. We observe that for both PG and RG models almost take the same shape with a small difference. The entropy values obtained by the Real Gas model are always higher than those obtained by the Perfect Gas model for β>50°. The effect of the stagnation pressure P_0 is found to be very small and can be neglected. In this case, the error between the two models reach a value of 7.30% for a stagnation pressure P_0 of 1 bar (Table 1). This variation will influence the thermodynamic parameters of the encountered flow: (Bounjad *et al.* 2017, Bounjad, *et al.* 2017, Raltson and Rabinowitz 1985).

5.7 Variation of the Deflection Angle for a given upstream Mach number

Fig. 9 illustrates the results of the Deflection Angle (θ° in degrees) effect on the across OSW versus the upstream Mach number for certain stagnation pressures P_0=1 bar, 100 bar, and 500 bar and different values of oblique shock angle. As shown, the obtained curve has a parabolic form, and the gaps between the PG and RG models are more important when β is height.

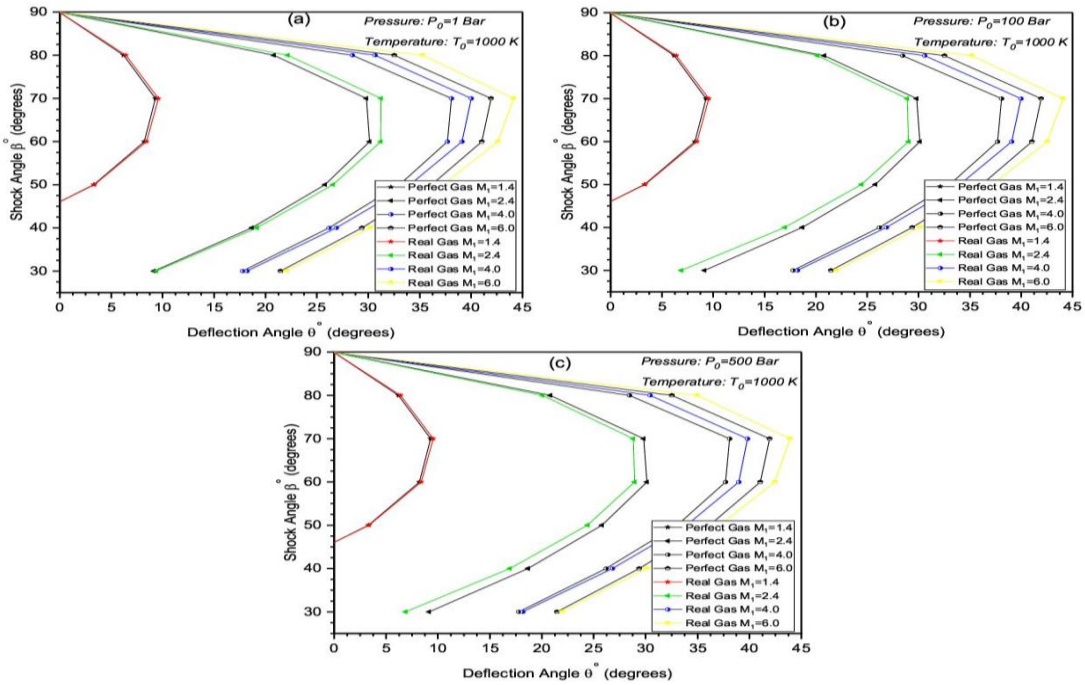

Fig. 10 Contours of M_1 for a given θ and β

For example if M_1<2.00 and β=30°, θ° is equal to -17.09015 for P_0=1 bar in case of the PG model, when θ° equal to -17.37541 for P_0=1 bar, -17.36707 for P_0=100 bar, and -17.34606 for P_0=500 bar, in the same conditions for RG model. If β=50°, θ° will be 3.298452 for the PG and θ°= 3.374813 for P_0=1 bar, 3.372567 for P_0=100 bar, and 3.36691 for P_0=500 bar, for RG model. If β=70°, θ° is equal to 9.291067 for the PG model, and θ°=9.580856 for P_0=1 bar, 9.572271 for P_0=100 bar, and 9.55066 for P_0=500 bar, for the RG model: (Tarnavskii 2004, Rodio *et al*. 2014).

Fig. 10 illustrates the contours of upstream Mach number M_1 for a given deflection angle θ° and shock angle β as well as certain stagnation pressures P_0=1 bar, 100 bar, and 500 bar, stagnation temperature T_0=1000 K. After calculation we can note that when $\theta<\theta_{max}$, there are two possible solutions for each value of the deflection angle θ, having two different wave angles. The larger value of β is called the strong shock solution, where the thermodynamic properties ratios are higher across the flow, and the smaller value of β is referred to as the weak shock solution, where the pressure, temperature, and density are less increased.

For the strong shock solution, the flow behind the shock becomes subsonic, whereas for the weak shock solution the flow behind the oblique shock remains supersonic. Any additional rise in deflection results in a bow shock divorced from the wedge, where the oblique shock theory is no longer valid. Higher deflection angles produce a larger shock (increases with) in the flow up to a maximum deflection: (Bounjad *et al.* 2017, Salhi and Roudane 2019, Salhi *et al.* 2016, Zebbiche 2019, Thompson 1995).

5.8 Error caused by the numerical process

The error represents the variation of the relative error given in percentage considering the two

Table 1 Numerical process error for oblique shock wave when M_1>1, T_0=1000 K and P_0=1 bar

ε(%)	β=30°	β=50°	β=70°	β=90°
$\varepsilon(\rho_2/\rho_1)$	3.60	6.30	7.41	7.71
$\varepsilon(T_2/T_1)$	5.01	8.24	9.59	9.96
$\varepsilon(P_2/P_1)$	1.21	1.42	1.47	1.48
$\varepsilon(P_{02}/P_{01})$	1.40	7.96	14.34	16.79
$\varepsilon(M_2)$	2.25	3.37	2.51	3.33
$\varepsilon(\Delta S_{2\text{-}1}/R)$	4.07	6.15	7.05	7.30

Table 2 Numerical process error for oblique shock wave when M_1>1, T_0=1000 K and P_0=100 bar

ε(%)	β=30°	β=50°	β=70°	β=90°
$\varepsilon(\rho_2/\rho_1)$	3.50	6.11	7.19	7.48
$\varepsilon(T_2/T_1)$	4.85	7.98	9.29	9.64
$\varepsilon(P_2/P_1)$	1.18	1.38	1.42	1.44
$\varepsilon(P_{02}/P_{01})$	1.35	7.70	13.87	16.23
$\varepsilon(M_2)$	2.19	3.27	2.43	3.22
$\varepsilon(\Delta S_{2\text{-}1}/R)$	3.95	5.97	6.85	7.09

Table 3 Numerical process error for oblique shock wave when M_1>1, T_0=1000 K and P_0=500 bar

ε(%)	β=30°	β=50°	β=70°	β=90°
$\varepsilon(\rho_2/\rho_1)$	3.23	5.65	6.64	6.91
$\varepsilon(T_2/T_1)$	4.47	7.33	8.53	8.85
$\varepsilon(P_2/P_1)$	1.09	1.27	1.31	1.32
$\varepsilon(P_{02}/P_{01})$	1.25	7.07	12.68	14.83
$\varepsilon(M_2)$	2.02	3.02	2.23	2.96
$\varepsilon(\Delta S_{2\text{-}1}/R)$	3.65	5.52	6.33	6.56

models PG model and the RG models. Tables 1-3 show the error for T_0=1000 and M_1>1. The main objective is to evaluate all flow parameters calculated for the oblique shock wave for different P_0, T_0 and β values. At low pressure, for β=50° and 70°, the error in the pressure ratio (P_{02}/P_{01}) is about 7.96% and 14.34%, Table 1, respectively. At height pressure, the error range from ε=7.07% to 12.68%.

Concerning the temperature ratio (T_2/T_1), at low pressure the error can reach a maximum value of 8.24% for β=50°, and 9.59% for β=70°, Table 1. At height pressure, the error is slightly in the same order (between 7. 98% and 9.29%), Table 2. At very height pressure (P_0=500) and height temperature the maximum error is about (7.33% and 8.53%), Table 3.

In case of the Entropy ($\Delta S_{2\text{-}1}/R$), the error reach a value of 6.15%, 5.97%, and 5.52% for β=50°, P_0=1 bar, 100 bar and 500 bar, Tables 1-3 respectively, the error varies from 7.05%, 6.85% and 6.33%. In the case of β=70° (to see Tables 1-3), the maximum error is about 7.05% for P_0=1 bar.

The error in the pressure ratio (P_2/P_1) is very small equal to 1.42%, 1.38% and 1.27% for β=50°, P_0=1 bar, 100 bar and 500 bar, Tables 1-3 respectively, where ε=1.47%, 1.42% and 1.31% for the same pressure and β=70°, Tables 1-3: (Zebbiche 2009, Elaichi and Zebbiche 2018, Bounjad *et al.* 2017, Bounjad, *et al.* 2017, Raltson and Rabinowitz 1985).

We remark that the error is small, it can lead to non-adaptation of the air intake, since the

thickness of the shock wave is very small. We note that the error increases with increasing β requiring the use of RG model. For low values of P_0 and β, the PG model gives good results. The limit to use the PG model depends on the accuracy required.

6. Conclusions

In this study, we followed a new approach, which consists in reformulating all the known equations of the oblique shock waves in case a Perfect Gas to Real Gas. In order to see the behavior of the latter and subsequently propose a new mathematical model dependent on certain local flow conditions. These results are available only for the case of a perfect gas with constant specific heats C_P and a constant γ ratio. In particular, we have highlighted the proposed *RG* model and compared it with the *PG* model, calling the classical model. To this end, several conclusions were reached from this study, which is mentioned below:

- The work carried out can be considered as a numerical wind tunnel.
- It enables numerical validation of the new RG model against the experimentally validated old PG model.
- If the error is lower than 5%, which is generally accepted for aerodynamic applications, an oblique shock wave can be studied by using the equations of a perfect gas. This is applicable, when T0 is less than 1000 K for any upstream Mach number value, or when the Mach number is less than 2.
- The introduction of the Real Gas model requires the resolution of a system of nonlinear algebraic equations with the derivation or integration of complex analytical functions, which requires numerical programming and data processing with important computing time. Unlike the model perfect gas, this is represented by an explicit and simple equation and does not require significant computing time.
- The equations of the Perfect Gas model can be obtained by starting from the real gas, and by cancelling the intermolecular force, the molecular size, and the molecular constant of vibrational energy. In this case, the Perfect Gas model becomes a particular case of the Real Gas model.
- At low pressure, temperature, shock angle β, and Mach number, the differences in results between the two models of gas can be neglected. This provides the advisability of studying the flow of the Real Gas model by using the equations of the Perfect Gas model. However, as $T0$, shock angle β, and $M1$ increase, the resulting ideal gas separates from the real gas, so it is necessary to use the Real Gas model.
- The developed numerical program can process any gas found in nature. In this case, we must add the variation of the specific heat *CP* and the constant *R* of the gas to the calculation of *RG*.
- The convergence of the results requires an additional calculation time for the *RG* model compared to the *PG* model for the same accuracy.

As a perspective, we can study our problem through the use of *CFD* or even perform experimental tests on supersonic flow. Our study is established for the air, but it could be generalized for other fluids, the equations would remain valid. However, it would also be necessary to determine the intermolecular force, the molecular size, and the vibrational molecular energy constant.

References

Agnone, A.M. (1994), "Approximations for weak and strong oblique shock wave angles", *AIAA J.*, **32**(7), 1543-1545. https://doi.org/10.2514/3.12233.

Ali, A.H. (2023), "Numerical study of oblique shock wave", *Basrah J. Sci.*, **41**(1), 83-95.

Anderson, J.D. Jr. (1989), *Hypersonic and High Temperature Gas Dynamics*, McGraw-Hill Book Company. New York.

Anderson, J.D. Jr. (1982), *Modern Compressible Flow: With Historical Perspective*, McGraw-Hill, New York.

Bounjad, M. and Zebbiche, T. (2017), "High temperature gas effect on the normal shock wave parameters", *Int. J. Mech. Product. Eng.*, **5**(10).

Boun-jad, M., Zebbiche, T. and Allali, A. (2017), "Gas effect at high temperature on the supersonic nozzle conception", *Int. J. Aeronaut. Space Sci.*, **18**(1), 82-90. http://doi.org/10.5139/IJASS.2017.18.1.82.

Boun-jad, M., Zebbiche, T. and Allali, A. (2017), "High temperature gas effect on the supersonic axisymmetric Minimum Length Nozzle design", *Int. J. Eng. Tech. Res.*, **7**, 23-30.

Boun-jad, M., Zebbiche, T. and Allali, A. (2017), "Numerical study of gas effect at high temperature on the supersonic plug and expansion deflexion nozzles design", *Int. Res. J. Eng. Technol.*, **4**, 1480-1488.

Elaichi, T. and Zebbiche, T. (2018), "Stagnation temperature effect on the conical shock with application for air", *Chin. J. Aeronaut.*, **31**(4), 672-697. https://doi.org/10.1016/j.cja.2018.02.009.

GaoXiang, X., Pengfei, Y., HongHui, T. and ZongLin, J. (2020), "Cellular aluminum particle-air detonation based on realistic heat capacity model", *Combus. Sci. Technol.*, **192**(10), 1931-1945. https://doi.org/10.1080/00102202.2019.1632298.

Goldsmith, E.L. and Seddon, J. (1999), *Intake Aerodynamics*, 2nd Edition, Blackwell Science.

Gupta, N. and Sharma, V. D. (2017), "Dissipative waves in real gases", *Int. J. Nonlin. Mech.*, **95**, 242-247. https://doi.org/10.1016/j.ijnonlinmec.2017.06.010.

Kenneth, E.T. (1996), "Computation of thermally perfect properties of oblique shock waves", CR- 4749, NASA.

Kopal, Z. (1947), "Tables of supersonic flow around cones", Report No. 1, Massachusetts Institute of Technology, Cambridge, Mass.

Maccoll, J.W. (1937), "The conical shock wave formed by a cone moving at a high speed", *Proc. Roy. Soc. London. Ser. A-Math. Phys. Sci.*, **159**(898), 459-472. https://doi.org/10.1098/rspa.0083.

Navarro, I.C. (2019), "Quasi-one dimensional flow through a nozzle with a shock", University of California, Irvine.

Peterson, C.R. and Hill, P.G. (1965), *Mechanics and Thermodynamics of Propulsion*, Addition-Wesley Publishing Company Inc., New York.

Raltson, A. and Rabinowitz, A. (1985), *A First Course in Numerical Analysis*, McGraw-Hill, US.

Rodio, M.G., Congedo, P.M. and Abgrall, R. (2014), "Two-phase flow numerical simulation with real-gas effects and occurrence of rarefaction shock waves", *Eur. J. Mech.-B/Fluid.*, **45**, 20-35. https://doi.org/10.1016/j.euromechflu.2013.11.007.

Salhi, M. and Roudane, M. (2019), "Numerical investigation of the thermal-caloric imperfections on entropy enhancement across normal shock waves", *High Temper.-High Pressur.*, **48**(4). 285-308. http://doi.org/10.32908/hthp.v48.689.

Salhi, M., Zebbiche, T. and Mehalem, A. (2016), "Stagnation pressure effect on the supersonic flow parameters with application for air in nozzles", *Aeronaut. J.*, **120**(1224), 313-354. https://doi.org/10.1017/aer.2015.13.

Sims, J.L. (1964), "Tables for supersonic flow around right circular cones at zero angle of attack", NASA SP-3004.

Sutton, G.P. and Biblarz, O. (2010), *Rocket Propulsion Elements*, 8th Edition, John Wiley and Sons.

Tarnavskii, G. A. (2004), "Influence of flow angularities in a hypersonic ramjet diffuser on the formation of the shockwve structure of the real gas flow", *J. Eng. Phys. Thermophys.*, **77**(3), 651-662.

https://doi.org/10.1023/B:JOEP.0000036514.14795.95.
Tatum, K. and Tatum, K. (1997), "Computation of thermally perfect oblique shock wave properties", *35th Aerospace Sciences Meeting and Exhibit*, 868.
Thompson, A.P. (1995), *Compressible Fluid Dynamics*, McGraw-Hill, US.
Van Wylen, G.J. (1973), *Fundamentals of Classical Thermodynamics*, John Wiley and Sons, US.
Zebbiche, T. (2009), "Effect of the stagnation temperature on the normal shock wave", *J. Comput. Meth. Sci. Eng.*, **9**(1-2), 79-92. https://doi.org/10.3233/JCM-2009-0253.
Zebbiche, T. (2019), "Stagnation pressure effect on the supersonic minimum length nozzle design", *Aeronaut. J.*, **123**(1265), 1013-1031. https://doi.org/10.1017/aer.2019.42.
Zebbiche, T. and Youbi, Z. (2006), "Effect of stagnation temperature on the supersonic flow parameters with application for air in nozzles", *Int. J. Aeronaut. Space Sci.*, **7**(1), 13-26. https://doi.org/10.5139/IJASS.2006.7.1.013.

AP

Notation

M : Mach number
P : Pressure
R : Thermodynamic constant of gas
S : Entropy
T : Temperature
V : Velocity
C_P : Specific heat at constant pressure
C_V : Specific heat at constant volume
C_T : Constant determined by a constant temperature
S_V : Sound velocity
γ : Specific heat ratio
ρ : Air Density
$E^{(T)}$: First function for energy equation
$E^{(\rho)}$: Second function for energy equation
$S^{(T)}$: First function for entropy equation
$S^{(\rho)}$: Second function for entropy equation
β : Shock angle
θ : Deflection angle
ΔS : Entropy jump
a : Constant of intermolecular forces
b : Constant of molecular size

Abbreviation

PG : Perfect gas
RG : Real gas
CFD : Computational fluid dynamics
OSW : Oblique Shock Wave
NSW : Normal Shock Wave

Subscripts

0 : Stagnation condition
1 : Parameter just before the shock wave
2 : Parameter just after the shock wave